Z. Phys. C 58, 77–93 (1993)

ZEITSCHRIFT
FÜR PHYSIK C
© Springer-Verlag 1993

J/ψ evolution and quark-gluon plasma to hadron phase transition*

J. Cugnon, P.-B. Gossiaux**
Université de Liège, Institut de Physique au Sart Tilman, Bâtiment B.5, B-4000 Liège 1, Belgium

Received 16 July 1992

Abstract. The influence of the internal motion of a $c-\bar{c}$ pair on the fate and on the evolution of this pair is studied by means of a Schrödinger model. The coupling of the $c-\bar{c}$ internal motion to the inelastic $D-\bar{D}$ channels is introduced through an imaginary potential. The effect of the change of the surrounding medium in which the $c-\bar{c}$ pair is travelling is assumed to be incorporated under the form of a time-dependent real potential. The model is studied for the case of a $c-\bar{c}$ pair leaving a plasma phase for a mixed phase and finally for free space. The time-dependent potential is thus assumed to extrapolate between the Debye-screened potential and the free space charmonium potential in a transition time τ. The influence of the initial wave packet and of the value of the transition time τ is particularly studied. We exhibit the time variation of global properties of the wave packet as well as of its components along the stationary states of the charmonium. We identify more or less two regimes: an expansion regime, which occurs for initially compact wave packets with large kinetic energy, where the wave packet spreads almost freely, and a compression regime, which occurs for broad initial wave packets, where the wave packet is basically compressed by the restoring confining potential. The influence of the imaginary potential is analyzed. The J/ψ and ψ' components are studied. It is shown that the former may be increased in some circumstances and that the latter may remain surprisingly large. The quantum character of these results is underlined.

1 Introduction

The so-called J/ψ reduction (as well as the ϕ-enhancement) has been considered as a possible signature of the existence of a quark-gluon plasma in the course of relativistic heavy ion collisions [1–4]. However, it is more and more clear that the data concerning J/ψ reduction can be explained by a rescattering of the J/ψ in a hadronic phase, be it composed of nucleons as in [5–7] or of pions as in [8–9]. The average $\langle p_t^2 \rangle$ and to some extent the p_t-dependence of the J/ψ yield require gluon rescattering prior to fusion in the frame of the fusion model for charm production. In order to distinguish between the two scenarios, one should probably wait for experiments performed at much higher energy: it is then expected that the p_t-dependence is not the same in the two scenarios [4].

In any of both approaches, the J/ψ is usually supposed to be structureless. Once it is created, it is considered to be an ordinary ("asymptotic") J/ψ, after some formation time perhaps in some works [2–3], and it is assumed either to stay in this state or to possibly disappear in some subsequent interaction. Our goal here is to remedy to this situation. We want to take account of the structure of the $c-\bar{c}$ wave packet and of its quantum-mechanical evolution when it is not in a pure state. To carry out this program, we adopt a very simple approach, though of good potentialities as we will see. As for the charmonium, we assume that the internal motion of a $c-\bar{c}$ pair may be described by a non relativistic time-dependent Schrödinger equation. The influence of the medium where the J/ψ is propagating is conveyed by the potential acting between the c and $\bar{c}$ quarks. In a plasma, it is basically the Debye-screened potential and in vacuum, it is the usual charmonium potential. The potential will depend on time for a changing environment.

Such a model has already been proposed in [10] (without the important feature of the coupling to the inelastic channels that we include here for the first time), where it is applied to the propagation of a $\bar{c}-c$ pair experiencing a Debye screened potential only, and where the influence of the asymptotic J/ψ state is particularly studied. Here, we will use this model in a situation where the confining potential between the c and $\bar{c}$ quarks is restored and which may be physically relevant at the end of the plasma phase. We will make a thorough inves-

* Work supported by contract SPPS-IT/SC/29
** Research Assistant, National Fund for Scientific Research (Belgium)

tigation of the model, paying much attention to the many aspects of the evolution of the wave packet in the physical case under consideration. We are furthermore primarily interested in two effects, never studied previously, namely the effect of a time dependent potential and the effect of the coupling to the inelastic channels. We postpone the analysis of the heavy ion data at the light of this model to a separate paper.

The paper is organized as follows. In Sect. 2, we present the model for the evolution of the $c-\bar{c}$ wave packet and describe how a real time-dependent potential can account for a situation where the $c-\bar{c}$ pair is moving inside a plasma which undergoes a phase transition to the hadronic phase. We also describe how the coupling to the inelastic channels can be introduced by a simple imaginary potential. In Sect. 3, we present our numerical results for the evolution of the global properties of the wave packet, like the rms radius and the average potential and kinetic energies. We show the interplay between the expansion of the wave packet and the action produced by the restoring confining force. We also discuss the evolution of the wave packet in terms of its components along the stationary states of the charmonium. In Sect. 4, we focus on the initial and final probabilities of finding a J/ψ or a ψ', and show that these probabilities can be increased or decreased by the evolution process, depending upon the initial conditions. Finally Sect. 5 contains our conclusion.

2 The model

2.1 General description

The internal motion of a $c-\bar{c}$ pair is assumed to be described by the following equation

$$i\hbar \frac{\partial \psi}{\partial t} = \left(-\frac{\hbar^2}{2\mu} \Delta + V(\mathbf{r}, t) + iW(\mathbf{r}) \right) \psi, \tag{2.1}$$

where $\mathbf{r}$ is the relative distance between the c and $\bar{c}$ quarks, and $\mu = m_c/2$ is the $c-\bar{c}$-reduced mass. The potential $V(\mathbf{r}, t)$ is the $c-\bar{c}$ potential energy, whose time dependence is assumed to reflect the nature and the effect of the surrounding medium wherein the $c-\bar{c}$ pair is travelling. A great deal of work with (2.1) concerning charmonium spectroscopy (in the static case and with $W(\mathbf{r}) = 0$) have established the well-foundedness of the model, justified also by the heavy mass of the charmed quarks. Finally, $W(\mathbf{r})$ is an imaginary part, whose form is described below, introduced to account for the loss of probability due to the coupling to the $D-\bar{D}$ channels, which so need not be described explicitly. In another work [11], we have shown that this imaginary part well reproduces the widths of the charmonium states above the $D-\bar{D}$ threshold. In the first approach, we keep W constant in time.

In this work, we will assume that the medium does not bring any anisotropic effect. Therefore, V and W depend upon r only and the partial waves decouple as in the charmonium. We nevertheless introduce spin-spin and spin-orbit tensor couplings but we disregard the off-diagonal tensor term, which is not important for charmonium states. We will be concerned here with the $^3S_1$ ("J/ψ") channel only. Introducing the reduced radial wave function $u(r, t)$, (2.1) becomes in this channel

$$i\hbar \frac{\partial u(r, t)}{\partial t} = \left[-\frac{\hbar^2}{2\mu} \frac{\partial^2}{\partial r^2} + V(r, t) + iW(r) \right] u(r, t). \tag{2.2}$$

The form of the imaginary potential $W(r)$ is chosen as in [11], in the spirit of the flux tube fragmentation model. If the flux tube between the c and $\bar{c}$ quarks is stretched too much, it is supposed to break into pieces and lead to the formation of a $D-\bar{D}$ pair. The quantity $W(r)$ should then represent the probability of breaking a flux tube of length r. In common fragmentation models, the probability may be a complicated function of the length and of the past history of the flux tube. Here, we simply consider that W should be different from zero for a sufficiently large value of r only. As in [11], the following simple choice is made:

$$\begin{aligned} W(r) &= 0, && r < L, \\ &= -W_0, && r > L, \end{aligned} \tag{2.3}$$

with $W_0 = 38$ MeV and $L = 1$ fm. These values roughly reproduce the widths of the high lying charmonium states.

Equation (2.2) has been solved numerically by the Crank-Nicholson method, starting at initial time with a given wave packet and imposing $u(r, t)$ to vanish at $r = 0$ and at some large but finite distance.

2.2 The physical case

The model outlined above can be applied to many different physical cases, corresponding to many different time-dependances of the function $V(\mathbf{r}, t)$. We chose here to exhibit the features of the model in only one case, which, however, has not been studied up to now. Since we have primarily in mind a quark-gluon scenario, we single out the situation when a $c-\bar{c}$ pair leaves the plasma and enters the hadronic phase, or is sitting in a plasma which undergoes a phase transition to the hadronic phase. In both cases, at the initial time, the potential between the c and $\bar{c}$ quarks will by the Debye-screened potential. Ultimately, the potential experienced by the $c-\bar{c}$ pair will be the full charmonium potential with the confining part. We will thus consider a time-dependent potential interpolating continuously between the two situations, in a finite time interval:

$$V(r, t) = V_{\mathrm{OGE}}(r)\, e^{-\mu(t) r} + \left(1 - \frac{\mu(t)}{\mu_{\max}} \right) K r, \tag{2.4}$$

where V_{OGE} is the one-gluon exchange part of the static $c-\bar{c}$ potential, K is the so-called string tension and

where $\mu(t)$ is taken as

$$\mu(t)=\left(1-\frac{t}{\tau}\right)\mu_{\max}. \tag{2.5}$$

The quantity $\mu_{\max}$ can be considered as the mass parameter corresponding to the Debye screening prevailing inside the plasma. In the following, we chose $\mu_{\max}=0.6$ GeV, according to [12]. For both V_{OGE} and K we adopted the Richardson's parameters [13]. The quantity τ can be viewed as the time required for the phase transition to be complete, or more precisely, as the time after with the full charmonium potential is restored. We do not pay too much attention to its numerical value for the moment and we will present calculations for different values of this parameter.

To complete our model, we have to provide the initial conditions. We will take

$$\psi(\mathbf{r},t)=\frac{u(r,t)}{r}=A_0\exp\left[-\left(\frac{r-r_0}{\sigma}\right)^2\right], \tag{2.6}$$

where A_0 is the normalization constant. If $r_0=0$, one has a purely Gaussian packet, but we allow $r_0\neq 0$ to make a more general study of the model, and in particular to study the case of a $c-\bar{c}$ pair with well separated quarks. One may expect that at the end of the plasma phase, one can find two reasonably separated quarks with a relative momentum uncorrelated to their inter-distance. This cannot be described with a purely Gaussian wave packet ($r_0=0$), for which the average momentum is uniquely determined by the average inter-distance.

For later purpose, we will denote the charmonium Hamiltonian as

$$H_0=T+V_0, \tag{2.7}$$

where T is the kinetic energy and where V_0 can be written as

$$V_0(\mathbf{r})=V(\mathbf{r},\tau), \tag{2.8}$$

with the notation of (2.4).

3 Numerical results

3.1 Alternative parametrization of the initial wave packet

Instead of using the parameters r_0 and σ, we found more interesting in some cases to discuss the results in terms of the initial rms radius and the initial kinetic energy (formulae are given in Appendix 1) or the initial total

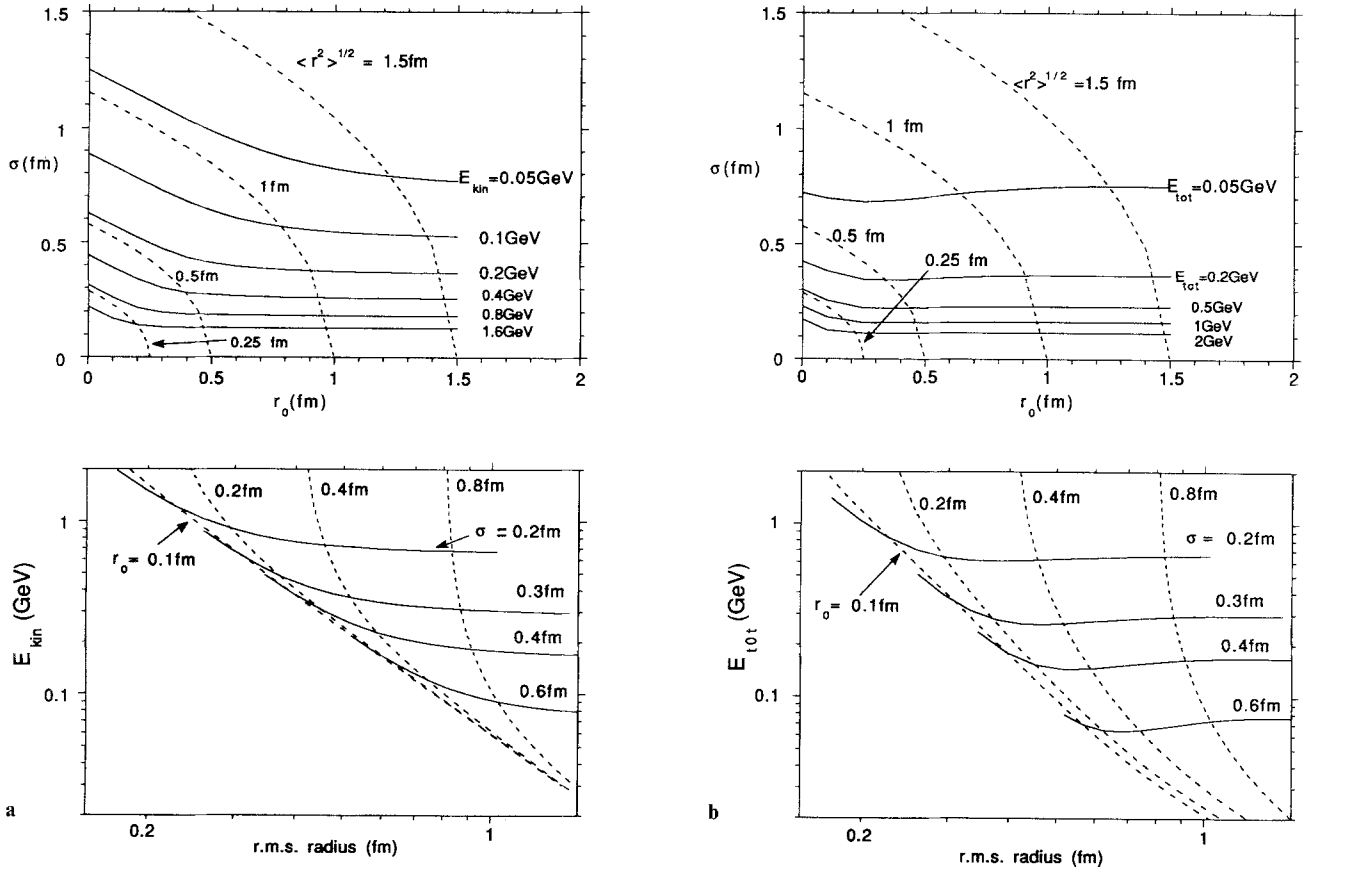

Fig. 1. a Upper part: curves of equal kinetic energy E_{kin} (full lines) and equal root mean square radius (dotted lines) for the wave packet (2.6). Lower part: curves of equal values of the parameters r_0 (dotted lines) and σ (full lines) for a wave packet of type (2.6) in the plane (kinetic energy (E_{kin}), root mean square radius). **b** Same as **a**, but using the total energy E_{tot} instead of the kinetic energy E_{kin}

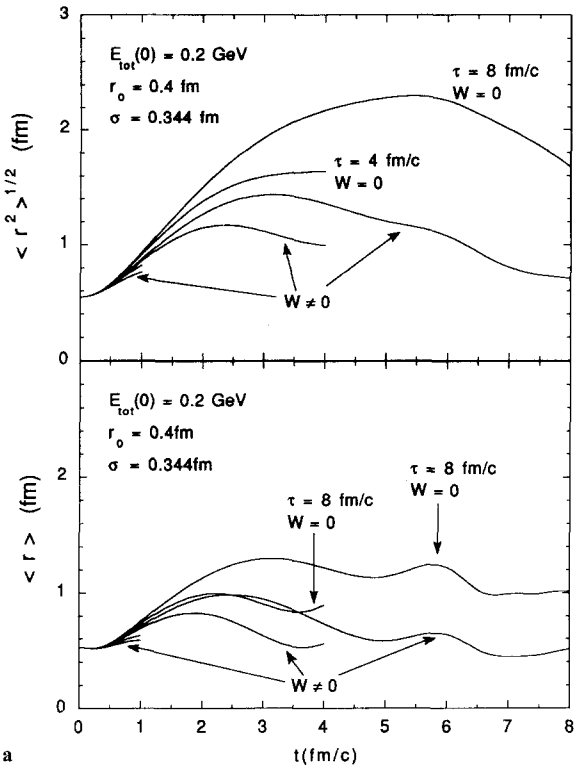

a

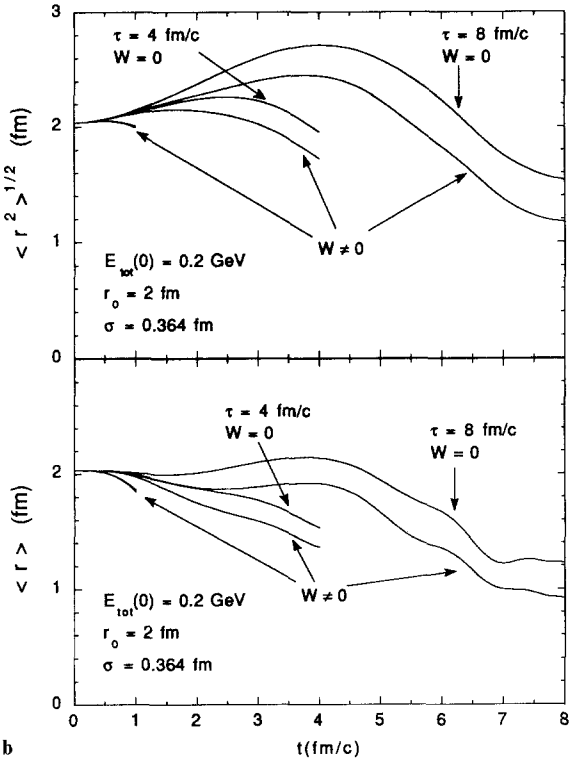

b

Fig. 2. a Time variation of the root mean square radius (upper part) and of the mean value of r (lower part) for an initial wave packet of indicated parameters, for three values of τ (1, 4 and 8 fm/c). In each case, the calculation is done with an imaginary potential of type (2.3) and with a vanishing imaginary potential. **b** Same as a, for an initial wave packet of type (2.6) with $r_0 = 2$ fm and $\sigma = 0.364$ fm

(kinetic + Debye screened potential) energy. The relations are illustrated in Fig. 1. Although the introduction of the parameter r_0 allows to handle wave packets with kinetic energy and rms radius which are not automatically linked, as it is the case for pure gaussian ones, it is not possible to have in this representation a wave packet with arbitrarily small values of the kinetic energy E_{kin} and of the rms radius (see bottom of Fig. 1). This is of course forbidden by the Heisenberg uncertainty principle. It is reminded that the limit consistent with this principle is realized for the pure Gaussian wave packets (see Appendix 1). The value of the total energy E_{tot} is significantly different (smaller) from E_{kin} for small values of r_0 and relatively small values of E_{kin}, only.

We will first study the global properties of the wave packets. As we will see, this is helpful for the analysis of their various components.

3.2 Time evolution of the rms radius

As an illustrative example, we take an initial wave packet with $r_0 = 0.4$ fm and $E_{\text{tot}}^{\text{in}}$ (the initial value of the total energy) $= 200$ MeV, i.e. with $\sigma = 0.344$ fm. The time evolution of the rms radius is given in Fig. 2 for several values of the transition time τ. For a very short τ, the rms radius slightly increases. For large values of τ, the rms radius starts to increase with a rate which is almost independent of τ and then further decreases. This behaviour is explained as follows: the initial expansion of the wave packet is dictated by the average kinetic energy and the further inflexion and decrease of the rms radius for large τ is due to the slowing down and the subsequent compression of the wave packet produced by the restoration of the linear confining potential. In fact, the physical situation is close to the one of a particle moving in a potential increasing linearly in time ($V = \dot{V}t$), for which it is possible to derive an analytic formula for the evolution of the root mean squared radius at small time (see Appendix 2). For a real initial wave packet, it writes (disregarding the imaginary potential)

$$\langle r^2 \rangle = \langle r^2 \rangle_0 + \frac{2}{m} \langle T \rangle_0 t^2 - \frac{1}{3m} \langle \mathbf{r}(\dot{V}\dot{V}) \rangle_0 t^3 + \ldots, \qquad (3.1)$$

where the symbol $\langle \ \rangle_0$ stands for the average of the operator over the initial wave packet and where T is the kinetic energy operator. If we consider the special case of a confining potential restoring linearly in time

$$V(r, t) = K r \frac{t}{\tau}, \qquad (3.2)$$

we obtain

$$\langle r^2 \rangle = \langle r^2 \rangle_0 + \frac{2}{m} \langle T \rangle_0 t^2 \left(1 - \frac{2}{3} \frac{K \langle r \rangle_0}{\langle T \rangle_0} \frac{t}{\tau} \right) + \ldots. \qquad (3.3)$$

This simple formula embodies the time variation of the calculated rms radius (for $W = 0$). One observes indeed at small t an increase of $\langle r^2 \rangle$, which is closer and closer

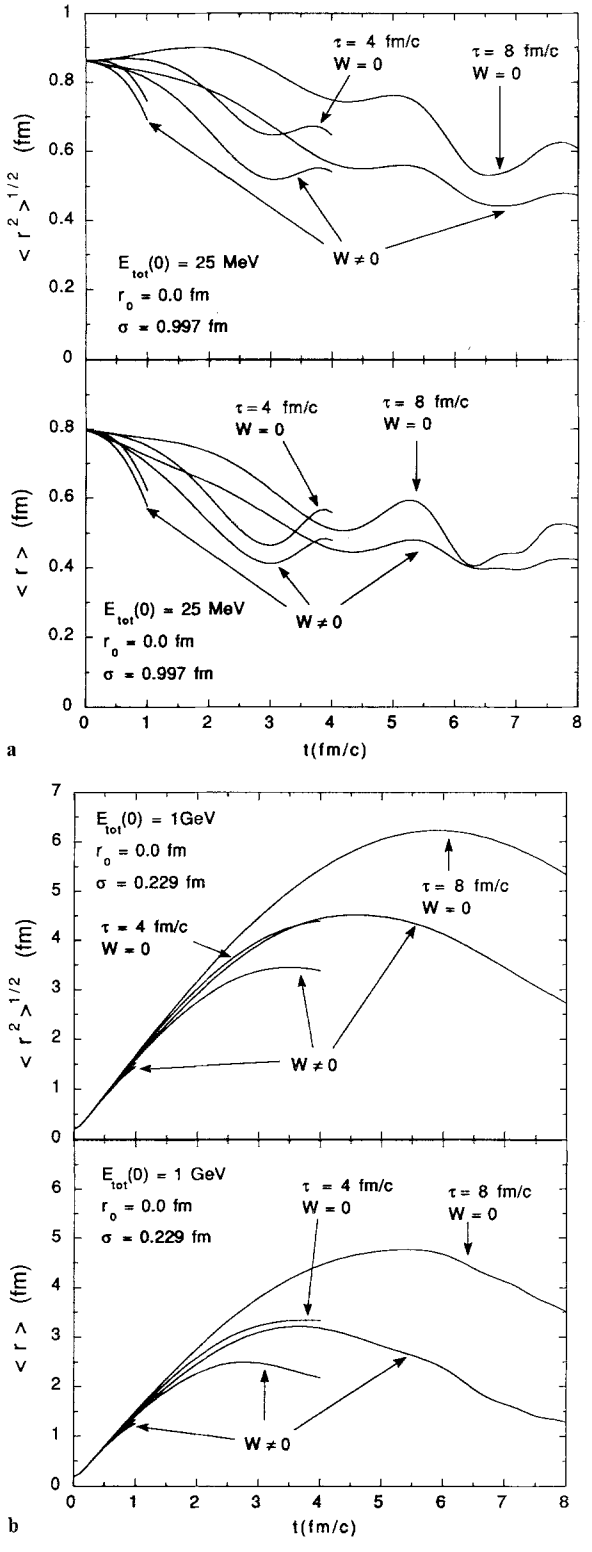

Fig. 3. **a** Same as Fig. 2a, for an initial Gaussian wave packet ($r_0=0$ and $\sigma=0.997$ fm). **b** Same as Fig. 2b, for an initial Gaussian wave packet ($r_0=0$ and $\sigma=0.229$ fm)

to the quadratic variation in t (exact for a free expanding real wave packet) for larger and larger values of τ. But for sufficiently large values of t (implying also a large τ), the cubic term in (3.3) eventually overwhelms the other ones. More precisely, one observes a decrease of the rms radius as soon as $\frac{t}{\tau} \gtrsim \frac{2}{3}\frac{K\langle r\rangle_0}{\langle T\rangle_0}$. This behaviour shows up in the next figures also.

A similar analysis can be done for the other illustrating case of Fig. 2b, which corresponds to $r_0=2$ fm, $E_{\text{tot}}^{\text{in}}=200$ MeV, or $\sigma=0.364$ fm. The behaviour is qualitatively the same as in the previous case. However the effect of the restoring confining potential is proportionally more important, since the initial wave packet has a larger extension. This is in keeping with the presence of the $\langle r\rangle_0$ factor in the last term of (3.3). For small τ, the restoring potential produces a small compression of the wave packet. For large τ, it is restored at a smaller pace: the wave packet has the time to spread before being compressed to a size smaller than the original one.

It is interesting to note that for a given time t, the rms radius is smaller for a smaller value of τ. This is once again dictated by the cubic term in (3.3). However one has to notice that the larger τ is, the smaller the final value of the rms is.

It is instructive to compare the time evolutions of $\langle r^2\rangle^{1/2}$ and $\langle r\rangle$, for the last case. The quantity $\langle r\rangle$ remains roughly constant when the rms radius is increasing. This means that the wave packet is spreading rather than expanding. In fact, our initial wave packet is real and there is no initial current. In the absence of forces, a wave packet as (2.6) with $r_0 \gg \sigma$ will spread and its $\langle r\rangle$ will remain close to r_0. On the other hand, if $r_0 \approx 0$ (as in Fig. 2a), the spreading of the wave packet will increase $\langle r\rangle$ for geometrical reasons.

The differences between the no absorption case and the absorption case result simply from the fact that the absorption gives rise to an attenuation of the wave function at large r, and thus to a reduction of the rms radius.

Figure 3 displays two typical situations of initial purely gaussian wave packet ($r_0=0$). In the first case, the initial rms radius is rather large since the kinetic energy is small. The general trend of the evolution is then a decrease of the rms radius, which is proportionally faster for smaller τ, in accordance with (3.3). For $\tau=4$ and 8 fm/c, one observes oscillations, which correspond to the fact that the wave packet is first compressed, "bounces" on $r=0$, expands and is further recompressed, and so on. This behaviour goes beyond the first terms of expansion (3.3). In the second case, the initial rms radius is very small ($E_{\text{tot}}^{\text{in}}=1$ GeV, $\sigma=0.23$ fm) and thus the initial kinetic energy is large. Therefore, the behaviour in this case is dominated by the free expansion, corresponding to the dominance of the second term of (3.3), for sufficiently small time at least. Note that the linear shape of the beginning of the curves in Fig. 3b results from the fact that $\langle r^2\rangle_0$ is very small and that the rms radius, and not $\langle r^2\rangle$, is plotted.

In all cases, for times larger than τ, the rms radius will continue to oscillate with however an overall damping (when $W\neq 0$), because of the continuous absorption, until it reaches a value ≈ 0.4 fm, corresponding to some mixing of the J/ψ and ψ' wave functions. The respective weights are of course given by the dynamic evolution. We stress that the time scale of the absorption

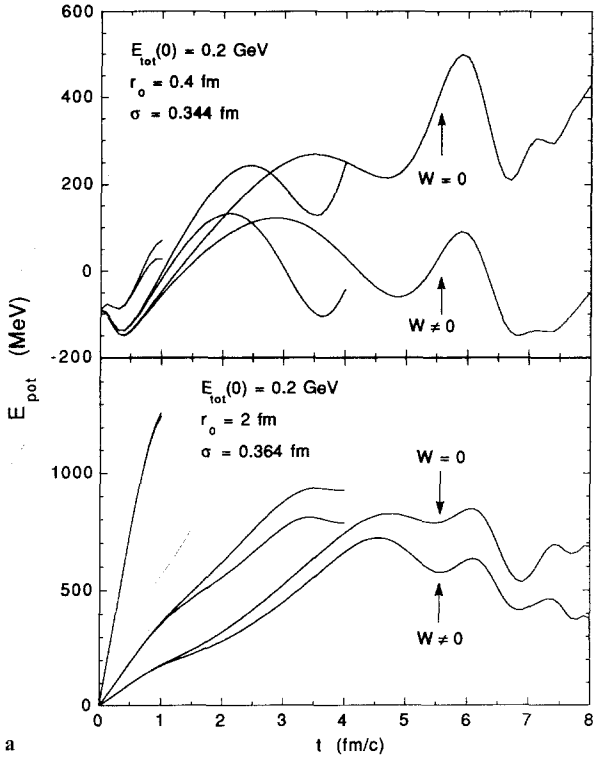

a

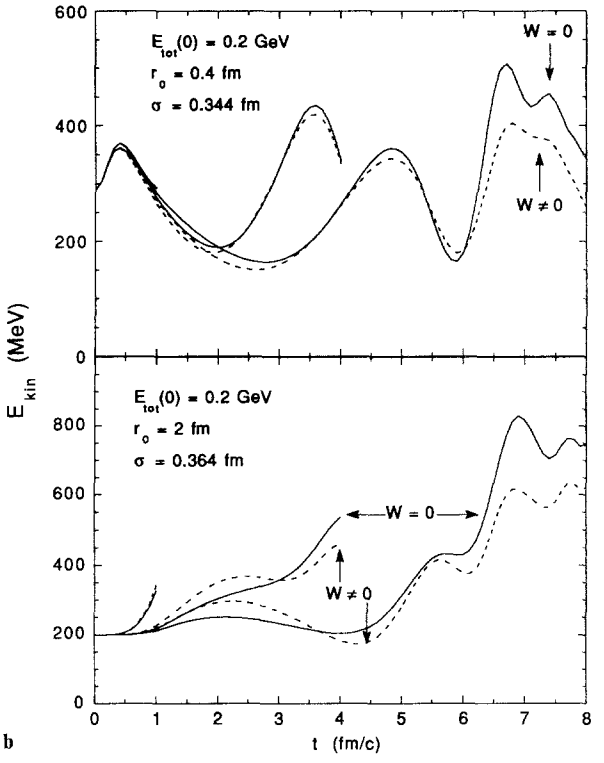

b

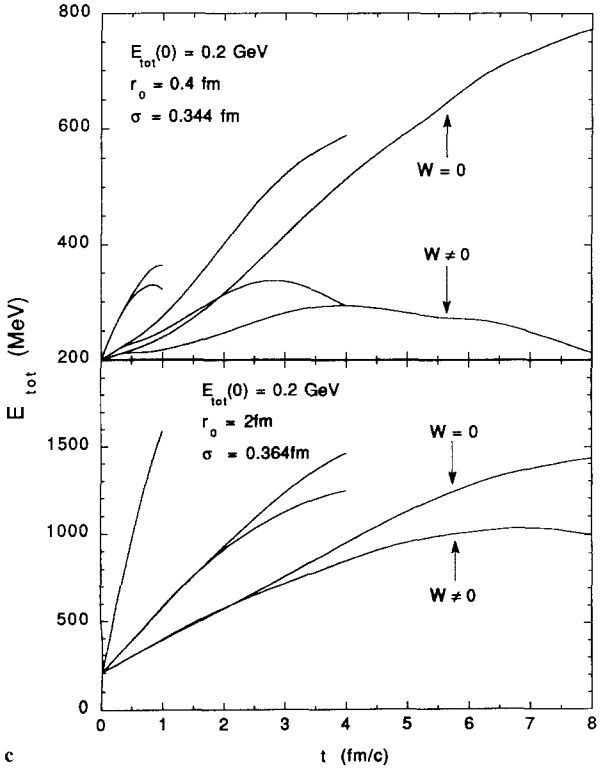

c

Fig. 4a–c. a Variation of the average potential energy for two initial wave packets: $r_0=0.4$ fm, $\sigma=0.344$ fm (upper part) and $r_0=2$ fm, $\sigma=0.364$ fm (lower part). In each case the calculation is done for three values of τ (1, 4 and 8 fm/c respectively) and for vanishing and non vanishing imaginary potentials. In each case the curve for $W=0$ lies above the corresponding curve for $W\neq 0$. **b** Variation of the average kinetic energy for the same cases as in a. The calculations for $W\neq 0$ are given by the dotted lines. **c** Variation of the average total energy for the same cases as in a. For the lower part and $\tau=1$ fm/c, the curves for $W=0$ and $W\neq 0$ are undistinguishable

$\left(\frac{\hbar}{W_0}\approx 5 \text{ fm/c}\right)$ is generally non negligible compared to, and sometimes larger than the time scale for the oscillations ($\approx$ a few fm/c's).

3.3 Time evolution of the average energy

We will concentrate here on the average values of the kinetic, potential and total energy of the $c-\bar{c}$ system, which are defined as

$$\langle E_i\rangle=\frac{\langle\psi|O_i|\psi\rangle}{\langle\psi|\psi\rangle}, \tag{3.4}$$

where $i=$kin, pot, tot and $O_i=K$, V_0 and H_0 (see (2.8)), respectively. The time evolution of these quantities is depicted in Fig. 4 for the same cases as in Fig. 2. The main effect is an increase of the potential energy. In fact, it can be shown that, for the case of a confining potential restored linearly in time and for an initial wave packet with zero mean momentum, the average potential varies as

$$\langle V\rangle = K\langle r\rangle \frac{t}{\tau} = \frac{K\langle r\rangle_0 t}{\tau} - \frac{K^2 t^4}{12 m \tau^2} + \mathcal{O}(t^5), \tag{3.5}$$

and that the kinetic energy varies as

$$\langle T\rangle = \langle T\rangle_0 + \frac{K^2 t^4}{12 m \tau^2} + \mathcal{O}(t^5), \tag{3.6}$$

the t^4 and higher order terms in both cases, coming from the corresponding variation of $\langle r\rangle$. These considerations explain why the gain in the potential energy in the second case is not the same for all values of τ. The longer τ is, the smaller the final value of $\langle r\rangle$ (see Fig. 2) is and the smaller the value of final potential energy is. In physical terms, the restoration of the confining potential raises the potential energy but, after some time, drives the wave function toward $r=0$. For the first case ($r_0=0.4$ fm), the situation is more complicated. The linear increase at low t corresponding to the first term of (3.5) is not clearly observed. This is so because for this initial wave packet the contribution of the Debye screened potential is not negligible at small t. This is also the reason why the initial potential energy is negative. For $t \lesssim 1$ fm/c, the variation of the potential energy does not follow at all (3.5). The slight minimum observed at $t \approx 0.4$ fm/c corresponds in fact to a small sliding of the wave packet inside the increasing Debye potential. Furthermore, in this case, one gains more and more potential energy for longer and longer τ. This occurs because of the increase of the final value of $\langle r\rangle$ with increasing τ (see Fig. 2).

Similar considerations help to understand the variation of the (average) kinetic energy (Fig. 4b). For $\tau=1$ fm/c, and $r_0=2$ fm, the wave packet hardly changes except for a small compression (see Fig.2b), which indicates the presence of an inward current and thus an increase of the kinetic energy (also in agreement with (3.6)). For larger τ's, the situation is qualitatively the same, but the inward global motion of the wave packet occurs later and is more pronounced. For the first case ($r_0=0.4$ fm) and $\tau=1$ fm/c, the kinetic energy does not change very much. The small bump is due to the Debye potential.

The slow decrease for t up to ~ 2 fm/c (for larger τ) is due to a slowing down of the global motion compared to free expansion, as is demonstrated in Fig. 2a. The further modifications are too involved to be described by simple considerations.

The variation of the total energy (Fig. 4c) can be understood on the basis of the following formula

$$\Delta E_{\text{tot}} = \frac{K}{\tau} \int_0^\tau \langle r\rangle(t)\, \mathrm{d}t, \tag{3.7}$$

which is nothing but as K multiplied by the time average value of $\langle r\rangle$, after inspection of Fig. 2.

We want to draw the attention on the influence of the Debye potential observed for $r_0=0.4$ fm, which can only show up in particular circumstances, when the initial wave packet is inside the Debye potential range with a small average kinetic energy.

Other typical cases, corresponding to initial purely gaussian wave packets are given in Fig. 5. They are both illustrative of the situation where the first term of (3.5) and (3.6) are rapidly dominated by the other terms. Actually, in the first case and for $\tau=1$ fm/c, the t^4 term can be clearly seen. In the first case, the dynamics is dominated by the effect of the restoration of the confining potential. This is particularly clear for $\tau=1$ fm/c, where the gain of the potential energy is no longer linear in time for $t \gtrsim \tau/2$: it is limited by a decrease of the size of the wave packet. The behaviour for the other values of τ (at least for the first part of the time interval) can be explained in the same manner, in concordance with the time evolution of the rms radius (see Fig. 3a). Similar considerations are sufficient to explain the behaviour of the average kinetic energy (Fig. 5b), which increases due to the inward motion of the wave packet.

The other case ($r_0=0$, $E_{\text{tot}}^{\text{in}}=1$ GeV, $\sigma=0.229$ fm) is dominated by the spreading of the initially compact wave packet. The potential energy increases steadily with time. Furthermore, the larger τ is, the larger the gain in potential energy is, because of a large spreading of the wave packet. Correlatively, the kinetic energy is steadily decreasing corresponding to a continuous slowing down of the wave packet for all values of τ. There is a little kink in all curves at $t \approx 0.2$ fm/c because the initially very compact wave packet starts to leave the Debye potential. The influence of the Debye potential is also reflected in the negative value of the initial potential energy. For broader initial wave packets, the effect of such a small detail in the potential is washed out.

From Figs. 4 and 5, we may draw the following conclusion. If one starts with a small kinetic energy or a large r_0, the evolution is dominated by the compression of the wave packet: therefore, the longer τ is, the smaller the average value of $\langle r\rangle$ is and the smaller the gain in total energy is, accordingly with (3.7). On the opposite, if one starts with a large kinetic energy or a small r_0, the characteristic evolution corresponds to the spreading of the wave packet: therefore, the longer τ is, the larger the average value of $\langle r\rangle$ is and the larger the gain in total energy is.

3.4 Time evolution of the wave function

The evolution of the wave function is much more complicated that the one of the global properties we just studied before. Therefore, we restrict ourselves to some illustrations.

The shape of the wave function at initial and final times is given in Fig. 6 for $r_0=0.4$ fm and $E_{\text{tot}}^{\text{in}}=200$ MeV (same case as top of Fig. 2). The most important feature is the appearance, for $W=0$, of oscillations at large r,

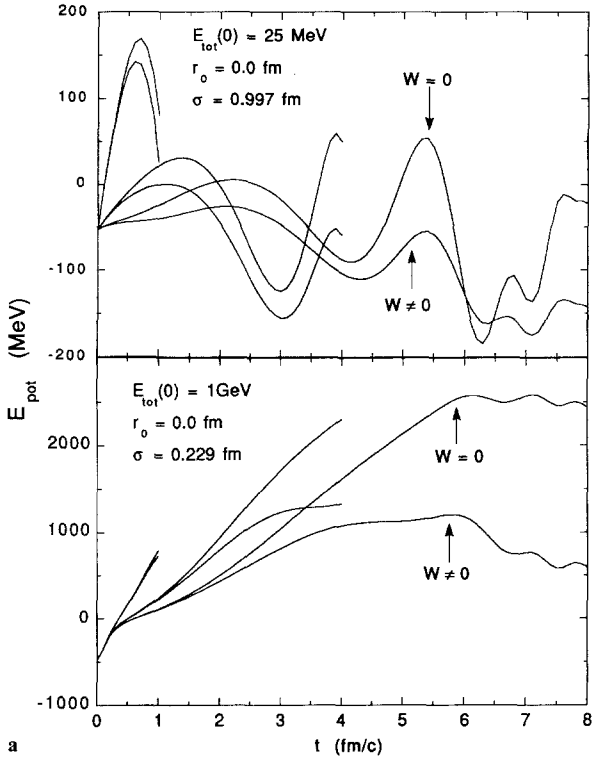

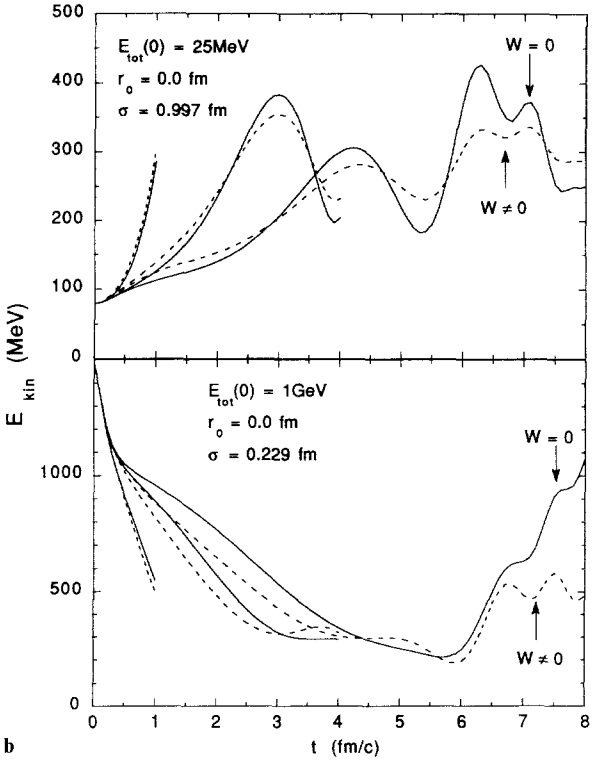

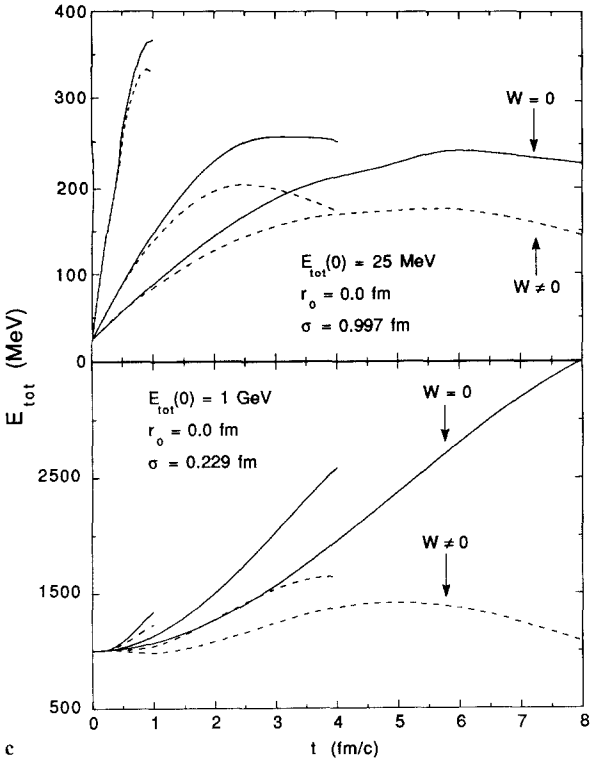

Fig. 5a–c. a Same as Fig. 4a for two Gaussian initial wave packets with $\sigma = 0.997$ fm (upper part) and $\sigma = 0.299$ fm (lower part). The curves for $W = 0$ are lying above the corresponding curves for $W \neq 0$. **b** Variation of the average kinetic energy for the same cases as in a. The calculations for $W \neq 0$ are given by the dotted lines. **c** Variation of the average total energy for the same cases as in a. The calculations for $W \neq 0$ are given by the dotted lines

which, of course, result mainly from the high momentum content of the initial wave function, but also from the interferences caused by the "reflection" of the wave function on the restoring linear potential. The effect of the imaginary potential is to damp the wave function for $r \gtrsim 1$ fm.

It is interesting to look at the components of the wave function along the stationary states of the charmonium Hamiltonian H_0 (2.7) (i.e. the real part of the Hamiltonian at final time). Their time evolution is depicted in Figs. 7 and 8, for two cases. The first case corresponds to a wave packet of a size similar to the one of the J/ψ with a relatively small average kinetic energy. The wave packet remains on the low components of the charmonium Hamiltonian, as indicated in Fig. 7. The components on the J/ψ and ψ' states remain important all

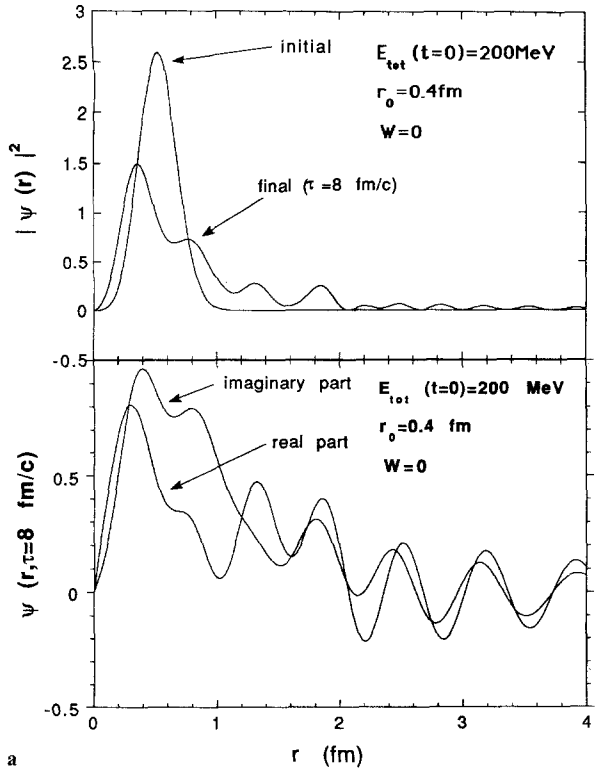

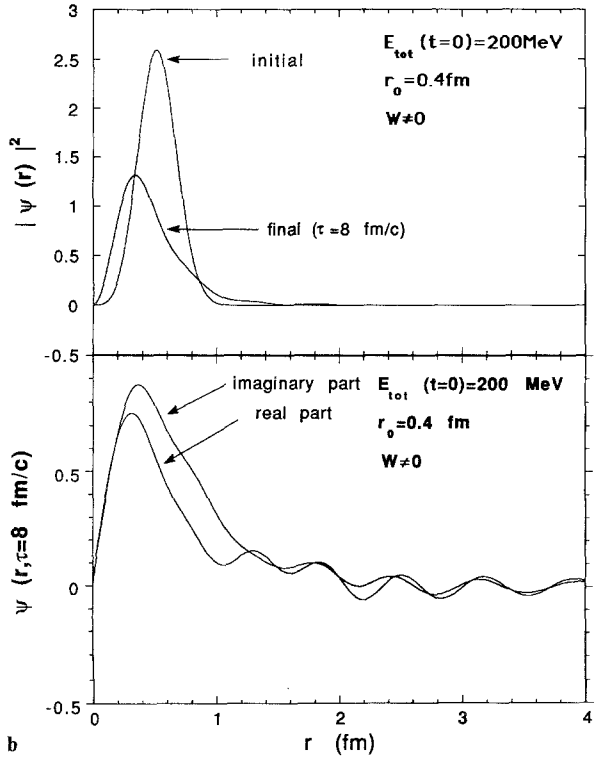

Fig. 6a–b. **a** Upper part: squared modulus of the initial wave packet ($r_0 = 0.4$ fm, $\sigma = 0.344$ fm) and of the final wave packet for $\tau = 8$ fm/c. Lower part: real and imaginary parts of the final wave function. The calculation is done for a vanishing imaginary part. **b** Same as a for the imaginary part of (2.3)

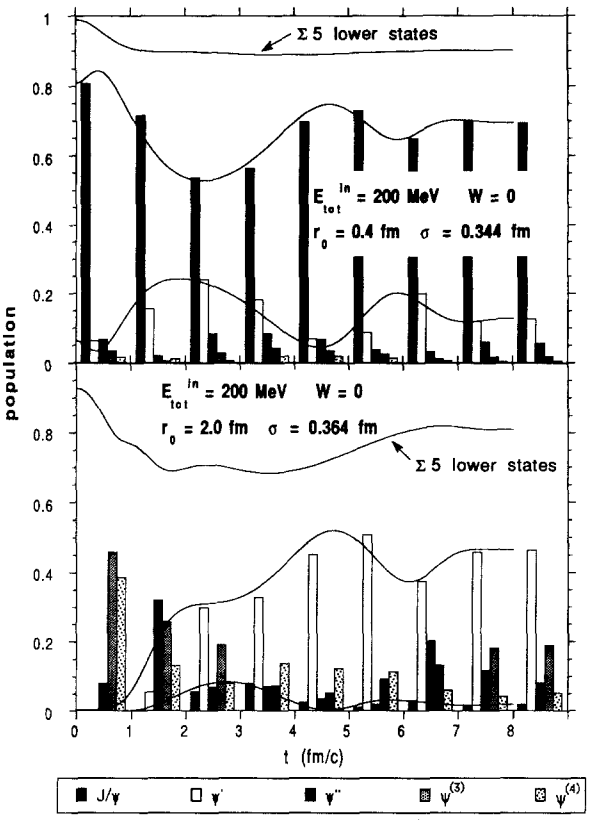

Fig. 7. The histograms give the (squared modulus of the) components of the wave function along the various stationary states of the real part of the charmonium Hamiltonian given at the bottom of the figure, for $t = 0, 1, 2, \ldots, 8$ fm/c. The upper part corresponds to an initial wave packet with $r_0 = 0.4$ fm and $\sigma = 0.344$ fm and the lower part, to $r_0 = 2$ fm and $\sigma = 0.364$ fm. The calculations are done with a vanishing imaginary part. To guide the eye, the time variation of the J/ψ and ψ' components is given by continuous curves. The norm of the wave function in the subspace spanned by the five lowest states is also given by continuous curves

the time. There is a typical (slightly damped) quantum oscillation between these states. In the second case, the initial wave function is much broader, the high energy component of the charmonium Hamiltonian are much more excited. There is an increase of the ψ' component, but the J/ψ one remains at a very low level.

The effect of the imaginary part is illustrated in Fig. 8: the most obvious effect is, of course, a continuous decrease of the norm of the wave function. But, from the inspection of Figs. 7 and 8, it is clear that the imaginary potential mainly cuts the high energy components. The physics is particulary transparent: when the wave function contains high energy (or momentum) components, it will expand easily and reach the absorption region, where the highest energy components will be progressively cut.

We also display in Figs. 9 and 10 the evolution of the components for the two cases studied in Fig. 3. In the first case, corresponding to a rather broad initial wave packet, the J/ψ component increases whereas the ψ' decreases. There is a quantum (damped) oscillation between these two coefficients, reminiscent of the two-

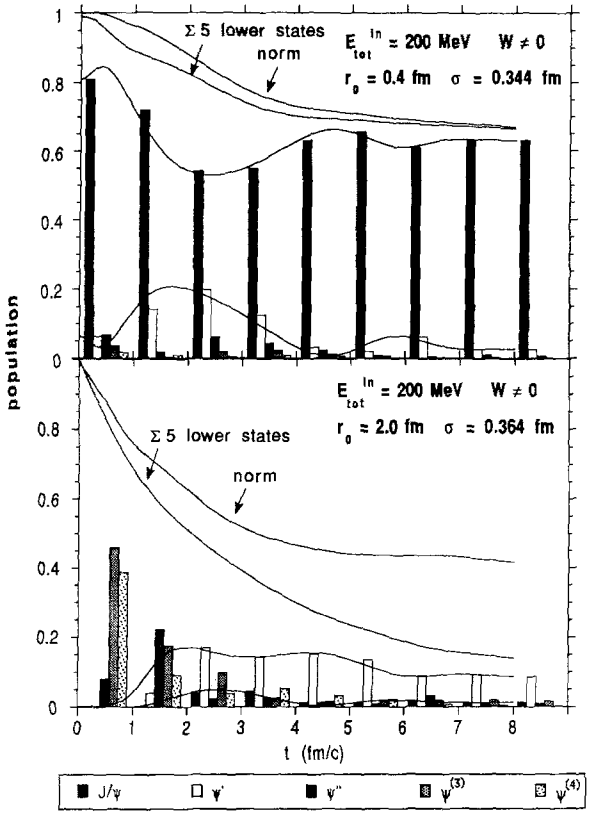

Fig. 8. Same as Fig. 7 with a non vanishing imaginary potential. The total norm of the wave function is also given by the upper curves in each case

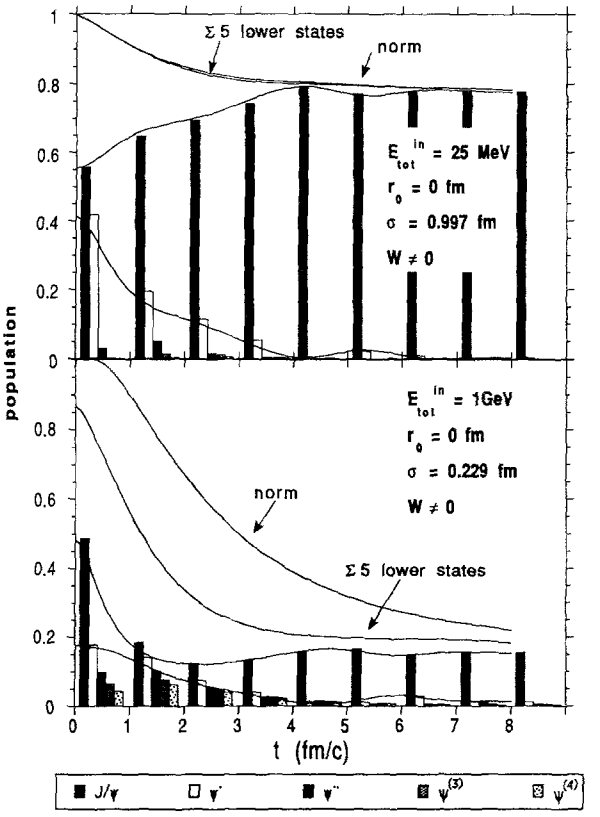

Fig. 10. Same as Fig. 9 for a non vanishing imaginary potential. The total norm of the wave function is given by the upper curve in each case

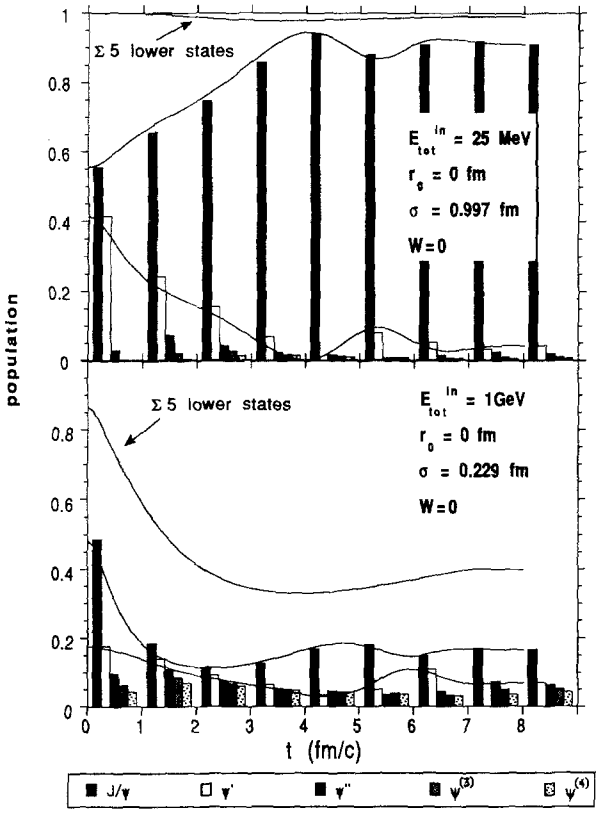

Fig. 9. Same as Fig. 7 for Gaussian initial wave packets with $\sigma = 0.997$ fm (upper part) and $\sigma = 0.229$ fm (lower part)

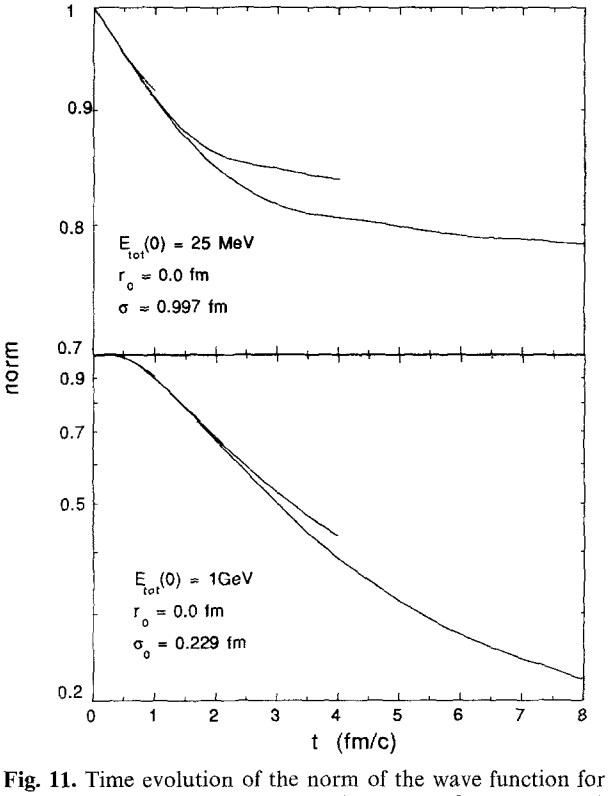

Fig. 11. Time evolution of the norm of the wave function for two Gaussian initial wave packets, with $\sigma = 0.997$ fm (upper part) and $\sigma = 0.229$ fm (lower part), and for $\tau = 1$, 4 and 8 fm/c

level case, similar to the one observed in Fig. 7. In the second case, corresponding to an initial wave packet of small size and with rather high momentum components, much more components along the charmonium stationary states are involved. As a matter of fact, the decrease of the J/ψ content is due to the overall population of higher energy components, as shown in Fig. 9.

The overall evolution of the J/ψ component in Figs. 9 and 10 can be understood in terms of overlapping wave packets (see Fig. 3). In the case of Fig. 9, the initial wave packet is somewhat broader than the stationary J/ψ, but its size slightly decreases as time evolves (Fig. 3). In the case of Fig. 10, the size of the wave packet rapidly reaches values which are much larger than the one of J/ψ. Therefore, the J/ψ content remains low. We have however to remind that these arguments based on geometrical overlap are not valid in general since the wave function may acquire rapidly varying phases. In the present context, they can be considered as provinding an upper limit for the J/ψ content. Figure 7 gives a clear illustration of these considerations since the J/ψ component has a very different intensity in both cases while the final size of the wave packet is rather similar (see Fig. 2).

It is remarkable that the final J/ψ abundance is not much affected by the presence of the imaginary part in the two cases illustrated in Fig. 10, despite the fact that the wave function is considerably modified, at least for the second case. The reason is that in both cases, the probability moves basically from the lowest states (J/ψ and ψ') to the higher states, as time goes on. An influence of the absorption potential could appear only when the J/ψ is populated from higher lying states (like for instance for an initial wave packet (2.6) with a large r_0, and as illustrated by the bottom of Figs. 7 and 8.

In conclusion, we have shown that the variation of the $c-\bar{c}$ potential can induce a large variation of the J/ψ, ψ' components. The total variation of those components can be understood in a qualitative way in terms of the global properties of the wave packet. However, we have shown that details of the variation are of purely quantum nature.

The time evolution of the norm is also illustrated in Fig. 11. It is interesting to note that in the first case the loss of norm seems to be limited: it is so because the restoring linear potential compresses the wave packet and tends to keep it confined within the region of space free of absorption. On the contrary in the second case, the large initial kinetic energy gives rise to a continuous expansion: the wave packet enters almost freely in the absorption region and the loss of norm is proportional to the outward flux, roughly proportional to the norm. This results as an almost exponential decrease with time.

4 J/ψ and ψ' final abundances

We now concentrate on the final J/ψ and ψ' abundances and study them as functions of the initial conditions and of the restoration time τ. We first consider a pure Gaussian wave packet ($r_0=0$). The results are contained in Fig. 12. For the J/ψ survival, there are two character-

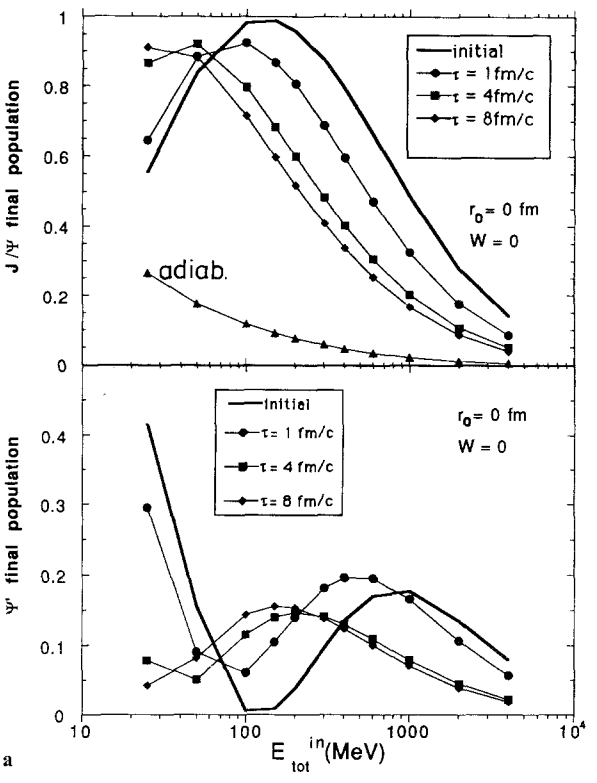

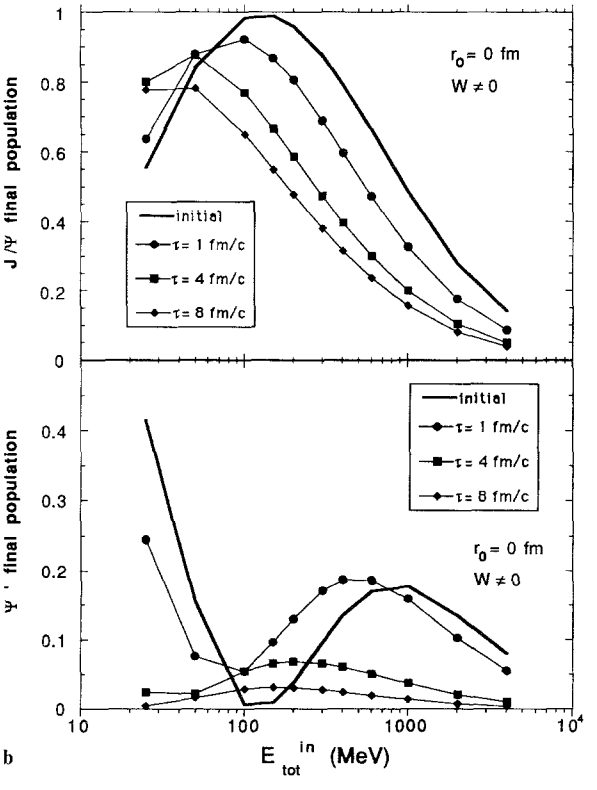

Fig. 12. **a** Upper part: initial and final J/ψ probability for gaussian wave packets ($r_0=0$) of various initial total energy $E_{\text{tot}}^{\text{in}}$. The calculations are done for various values of τ (1, 4 and 8 fm/c) and for a vanishing imaginary potential. The curve with the small triangles gives the adiabatic limit (see text). Lower part: same for the ψ' probability. **b** Same as a for a non vanishing imaginary part

istic regimes: one corresponding to a decrease, with increasing τ, of the J/ψ content, for $E_{\rm tot}^{\rm in} \gtrsim 100$ MeV and the other one corresponding to an *increase* of the J/ψ content, for $E_{\rm tot}^{\rm in} \lesssim 50$ MeV. The first regime is easy to understand in terms of overlapping wave packets: the initially compact wave packet is expanding and has thus little chance to resemble a J/ψ when times goes on. This is more and more true for increasing values of τ. On the other hand, for $E_{\rm tot}^{\rm in} \lesssim 50$ MeV, the initial wave packet is broader than the J/ψ, the restoration of the linear potential tends to make it alike. However, this reasoning does not seem to be valid for large values of τ. As a matter of fact, for larger and larger values of τ, one should approach the adiabatic limit. The latter may be discussed as follows. Let $\psi_{J/\psi}^{\rm ad}(t)$ and $E_{J/\psi}^{\rm ad}(t)$ be respectively the wave function and the energy of the stationary eigenstate of the *instantaneous* Hamiltonian $H(t)$ ((2.2), with $W=0$), which turns into the actual J/ψ when t is changed continuously into τ.

Let us consider the quantity

$$P_{\rm ad} = \lim_{\tau \to \infty} |\langle \psi(\tau) | \psi_{J/\psi} \rangle|^2, \tag{4.1}$$

where $\psi(\tau)$ is the wave packet at the end of the evolution and where $\psi_{J/\psi}$ is the actual J/ψ. The latter is also equal to $\psi_{J/\psi}^{\rm ad}(\tau)$. We can then write successively (for H real)

$$\begin{aligned} P_{\rm ad} &= \lim_{\tau \to \infty} |\langle \psi(\tau) | \psi_{J/\psi} \rangle|^2 \\ &= \lim_{\tau \to \infty} |\langle (e^{-i \int_0^\tau H(t)\,dt})^+ \psi(0) | \psi_{J/\psi}^{ad}(\tau) \rangle|^2 \\ &= \lim_{\tau \to \infty} |\langle \psi(0) | e^{+i \int_0^\tau H(t)\,dt} \psi_{J/\psi}^{ad}(\tau) \rangle|^2 \\ &= |\langle \psi(0) | \psi_{J/\psi}^{\rm ad}(0) \rangle|^2, \end{aligned} \tag{4.2}$$

since in the limit $\tau \to \infty$, the ket in the third line corresponds to the backward propagation in time of $\psi_{J/\psi}^{\rm ad}(\tau)$. The quantity $P_{\rm ad}$ is given in Fig. 12a by the small triangles. In our case, it is rather large at small energy (below 10 MeV) since our Debye-screened potential ((2.4) for $t=0$) accommodates a single weakly bound state, with a binding energy of a few MeV.

For continuity reason, whatever the value of $E_{\rm tot}^{\rm in}$ is, the J/ψ final probability should ultimately decrease toward the adiabatic value.

The final ψ' abundance is given in the lower part of Fig. 12a. The most remarkable feature is the minimum observed around 100 MeV total initial energy in the initial ψ' abundance: this occurs because the ψ' wave function has a node and thus the overlap with a Gaussian of a similar size leads to a cancellation associated with the maximum in the J/ψ component. Here, the behaviour of the final abundance is more involved, but one also clearly observes two depletion regimes bracketing a repopulation regime.

Comparison between Fig. 12a and b reveals that the imaginary part does not play a very important role for the J/ψ and for the ψ' abundance for small τ. In fact, our results show that it has a strong influence on the wave function when the total initial energy is very large only (see Fig. 11). In general, its net effect is to cut the high energy components and to reduce the norm, but not so much to perturb the J/ψ component. On the other hand, for low initial energy, the effect of the imaginary part on the high energy components and on the total norm is not very much important, but its effect on the J/ψ component is proportionally more important. This occurs because, in this particular case, the wave function mainly enters the absorption zone before being compressed to roughly the J/ψ size. Furthermore, the imaginary potential has the strongest influence on the ψ' component for large τ.

As another illustrative case, we consider a wave packet of the type of (2.6) with $E_{\rm tot}^{\rm in} = 200$ MeV and a variable initial value of rms radius, which, in this case (see Fig. 1), cannot be smaller than ~ 0.35 fm. The initial and final J/ψ and ψ' abundances are given in Fig. 13. Here again, we observe a depletion regime and a repopulation regime of the J/ψ. They can also be explained in terms of overlapping wave packets. A broad initial wave packet is reduced in size when the linear potential is restored and its overlap with the J/ψ wave function will be increased. On the other hand, if the initial wave packet is narrow, the main effect is a spreading of the wave packet and a decrease of the J/ψ component. Similar considerations can explain the ψ' component, which may be has high as 0.8. This behaviour is consistent with the expected continuity with the adiabatic limit (shown in Fig. 13a) when τ increases and tends to infinity. Finally, the imaginary part has some importance for large τ only, especially for the ψ' component.

A general view of our results is contained in Fig. 14. It shows the initial probability of finding a J/ψ in the initial state (upper part) and the ratio between final and initial probabilities (middle part), for a restoration time of $\tau = 8$ fm/c (and for $W=0$). The plane (r_0, σ) can be divided into two regions, corresponding to an increase or a decrease of the probability, respectively. Typically, low r_0 and low σ wave packets, i.e. compact wave packets with large kinetic energy correspond to a decrease of the J/ψ probability. These are typical of the expanding regime: the wave packet spreads very quickly and the overlap with the J/ψ is bound to decrease. On the other hand, very broad wave packets with small r_0 or very spiky wave packets with large r_0 and small σ or broad wave packets with large r_0 correspond to a decrease of the J/ψ probability. These are typical of the compression regime: the wave packet is expected to be compressed by the restoring potential and to resemble more and more to the J/ψ. It is remarkable that the dividing line in Fig. 14b corresponds to $\langle r^2 \rangle \approx 0.5$ fm^2.

We have shown the probabilities for $\tau = 8$ fm/c only, but we checked that the J/ψ final probability changes smoothly when τ is changed. Qualitatively, the final to initial probability plot remains the same for other values of τ.

In Fig. 14c, we plot the J/ψ final to initial probability ratio with absorption ($W \neq 0$). By comparing Fig. 14b and c, one may notice that the absorption has little effect in the expansion regime. This observation is not contra-

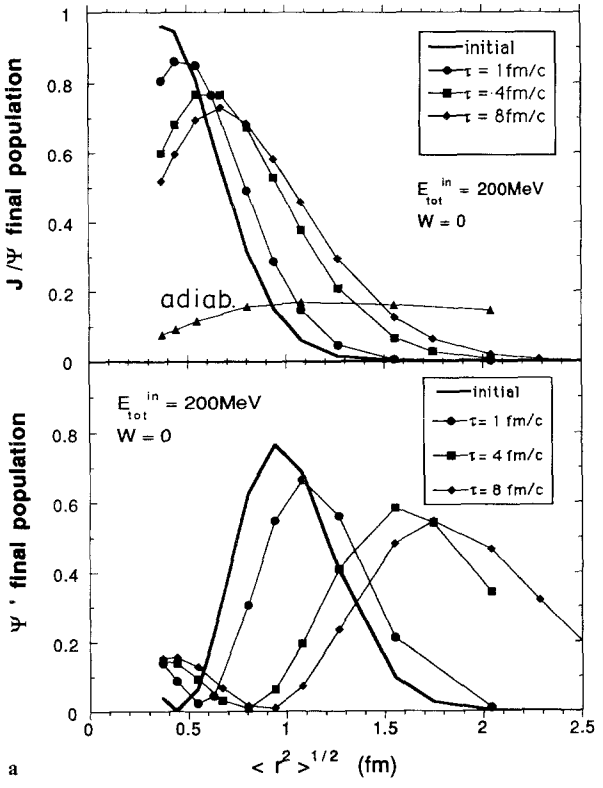

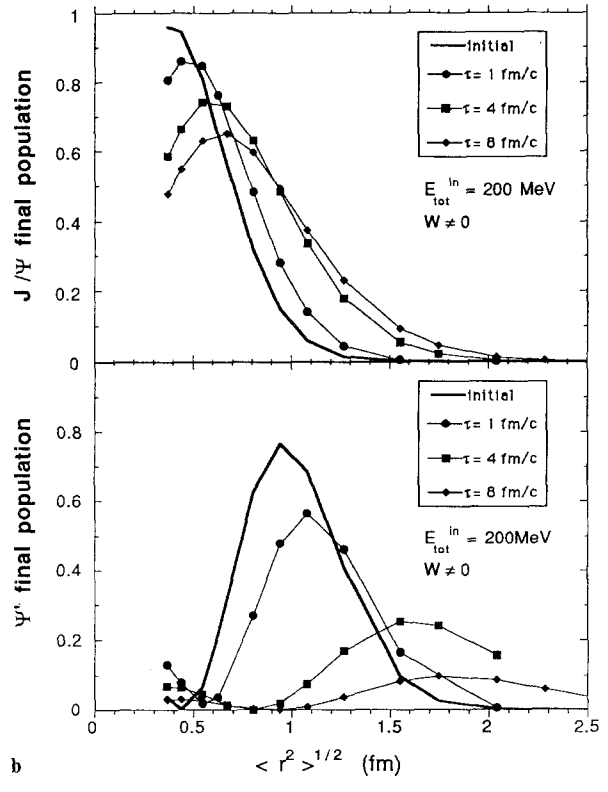

Fig. 13a. a Same as Fig. 12a for an initial wave packet of total initial energy E_{tot}^{in} of 200 MeV and for various values of the root mean squared radius (see Fig. 2). **b** Same as Fig. 12b for an initial wave packet of total initial energy E_{tot}^{in} of 200 MeV and for various values of the root mean squared radius (see Fig. 2)

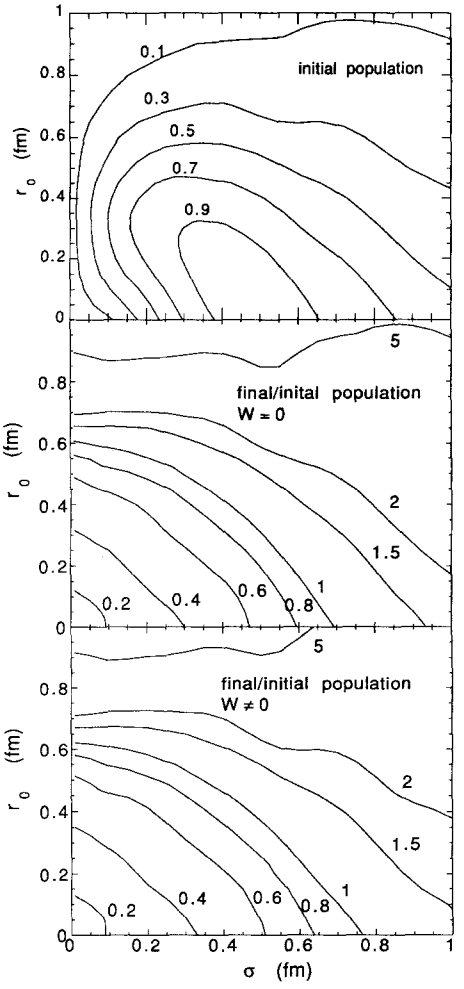

Fig. 14. Upper part: curves of equal initial J/ψ probability as a function of the parameters r_0 and σ (the values of the probability are given by the numbers). Middle part: curves of equal values for the ratio of the final to initial J/ψ probability for a vanishing imaginary potential W. Lower part: same as middle part for a non vanishing imaginary potential. The calculations are done for $\tau = 8$ fm/c

dictory with the strong effect of the absorption on the wave function in this regime (see Fig. 11 e.g.). In the latter, the wave packet is spreading very quickly. When $W \neq 0$ it is absorbed as soon as it penetrates the absorption zone. The spreading is so important (and basically one way) that its overlap with the J/ψ (at short distance) is not influenced by the behaviour at long distances.

The importance of the absorption in the compression regime is, as expected, more pronounced: one starts with a wave packet which is partially in the absorption zone.

It may be surprising that the absorption does not play a very important role for the J/ψ, at least in the range of the parameters shown in Fig. 14. However, one has to keep in mind that the absorption, because of its action at large r only, influences the high-energy components (i.e. those along the high-lying levels of H_0). Therefore the influence will be the strongest when one starts with a wave packet with high-energy components that are depopulated in favour of low-energy components in the dynamical process. This seems to happen for the

upper right corner of Fig. 14c. As a consequence, it is expected that in this regime the imaginary potential has a stronger influence on the ψ' final probability: that is what we observe in Fig. 13 for large rms radii.

5 Discussion

Our purpose here was to study the J/ψ propagation model described by (2.2) and to exhibit its dynamics in a particular example, but for quite general initial wave packets. We want to postpone the discussion of the implications of our model to the possible formation of the quark-gluon plasma in heavy ion collisions to a forthcoming publication, but we will examine some physical aspects of our results in the next section. We will here discuss the assumptions of the model.

Our model assumes a decoupling between the c.m. motion of the $c-\bar{c}$ pair and the internal motion. This seems to be reasonable in the high translational energy limit. However, this decoupling may be more general, since the $c-\bar{c}$ pair appears as a color dipole and therefore the translational motion is not modified (in non relativistic mechanics) if the color field does not change sizeably on a scale larger or of the order of the size of the dipole.

Similarly, we assume a decoupling of the partial waves of the internal motion. This seems reasonable for a plasma in view of the lattice calculations which indicate a strong reduction of the color forces without changing their rotational invariance. In a changing environment, this should be considered as a first approximation only.

We also made a linear approximation (2.5) for the time restoration of the confining potential. This has the great virtue that we were able, for this case, to derive analytic expressions for the early time variation of the global quantities (rms radius, energy, ...). There is no justification of taking a linear dependence. However, we checked that the results are not very sensitive to this dependence, provided the latter is smooth and such that one can still speak of a practical restoration in the given time interval τ.

We used a time-independent imaginary potential because of the lack of any indication (our model can easily handle a time-dependent imaginary potential). The time-dependence would be related to the modification of the $D-\bar{D}$ threshold in a changing environment. The latter is probably weak since the effective mass of the quark c is not expected to change. As an extreme case, one may consider that the coupling to $D-\bar{D}$ channels vanishes in the plasma. Consequently, one should start the calculations in this paper with $W=0$ at $t=0$. One can therefore consider our results as giving an upper limit for the effect of the imaginary part. In any case, this time-dependence would have a minor effect on the J/ψ probability (see Sects. 4 and 6).

Finally, we use a non relativistic treatment for obvious practical purposes. The latter may be questionable for the cases with large kinetic energy, at least. In those cases, the evolution of the global properties of the wave function will certainly be affected by a relativistic treatment. For instance, its possible expansion will be slower compared to our results. However, as far as the J/ψ content is concerned, the non relativistic approximation is probably good even in these cases. Indeed, the J/ψ probability is given by

$$P(t)=|\langle\psi_{J/\psi}|\psi(t)\rangle|^2. \tag{5.1}$$

In a relativistic treatment, one has

$$P(t)=|\langle\psi_{J/\psi}|U_R(t-t_0)|\psi(0)\rangle|^2 \tag{5.2}$$

$$=|\langle U_R(t_0-t)\psi_{J/\psi}|\psi(0)\rangle|^2, \tag{5.3}$$

where U_R is the relativistic evolution operator. This means that it is equivalent for calculating $P(t)$, to propagate $\psi(t)$ forward in time or to propagate $\psi_{J/\psi}$ backward in time. For this propagation, a non relativistic approximation is probably quite good as calculation of charmonium spectroscopy indicates. However, it is then important to have a very good J/ψ wave function, with the right high momentum components.

6 Conclusion

The importance of the internal motion on the fate of a $c-\bar{c}$ and on its J/ψ and ψ' content has been studied in a very similar model to our one in [10, 14, 15]. All these works used a Schrödinger approach similar to the one outlined in Sect. 2. However, none of them introduces the coupling to the inelastic channels. Furthermore, all of them study the propagation of a $c-\bar{c}$ pair in a plasma, either introducing a Debye-screened potential [10, 14] or a schematic harmonic oscillator potential [15]. In [15], it is shown that the J/ψ content decays continuously on a time scale characteristic of the "semi-classical" expectation for the formation time of a bound state. In a forthcoming work, we will analyze the heavy ion data in the light of the propagation of a $c-\bar{c}$ pair inside a plasma and a "restoring" phase, as described by our model.

We now comment on the physical results of our model for the case of a restoring confinement. One of our main and not obvious results is the fact that the J/ψ may be repopulated in the course of the transition. As indicated in Fig. 14, this occurs for low-energy, large wave packets whose evolution is dominated by the compression of the wave packet by the restoring potential. We have shown that, depending upon the parameters of the initial wave packet, many of our results are dominated by two regimes: the (quasi) free spreading of the wave packet (as for narrow, highly energetic wave packets and small τ) and the compression of the wave packet by the restoring confining potential (as for broad wave packets). Of course these regimes can be identified for the values of τ envisaged here. For much larger τ, the evolution would be more complex.

The basic parameters of the model are r_0, σ and τ. The relevant values of r_0 and σ should be determined in a specific model for the $c-\bar{c}$ formation. They however give rise to broadly varying effects even in the limited

range considered here that this deserves further investigations. The quantity τ represents the time necessary for the J/ψ to pass from the plasma to the hadron phase. This time should depend upon the evolution of the plasma itself and upon the relative velocity of the J/ψ with respect to the plasma. If one considers a J/ψ at rest with respect to the plasma, τ will be the intrinsic time required for the phase transition to be complete. There is very few information about the size of this quantity. In a particle model for the phase transition occurring in bulk matter, Knoll et al. [16] arrived at a time of the order of ~ 10 fm/c. This relatively long time is dictated by the fact that the phase transition should correspond to a strong decrease of the entropy density. In a bubble model for the transition, Csernaï et al. [17] arrived at about the same value. This value should be considered as an upper limit for our parameter τ, since the J/ψ may be moving with respect to the matter and therefore may "see" the transition in a smaller amount of proper time.

The imaginary potential W acts on the wave function for r larger than ~ 1 fm. In the parameter space, it is not easy to assess the importance of W. Although the norm of the wave function may be substantially attenuated (see Fig. 11), the imaginary part has a relatively small influence on the J/ψ content (see Fig. 14), except for broad initial wave packets. This may not be surprising since the absorption acts at "large" r only, and thus on the components along the high-lying stationary charmonium states only. Because of the same reason, the influence on the ψ' component should be much more important.

The possible repopulation of the J/ψ (see Figs. 13 and 14) and the time oscillations of the J/ψ amplitude (Fig. 10) clearly show the quantal nature of the J/ψ evolution. (A similar problem of the evolution of the wave packet under restoring confining walls was studied by [14] in the very crude case of a square well). The results of Figs. 13, 14 and the even the evolution of the norm could not be cast in a simple cross-section picture.

Appendix 1. Formulae related to the wave packet (2.6)

Let us consider the following wave packet

$$\psi(\mathbf{r}) = A \exp\left[-\left(\frac{r-r_0}{\sigma}\right)^2\right], \tag{A1.1}$$

normalized to unity. The quantity A is given by

$$A = \left\{4\pi\left(\frac{\sigma}{\sqrt{2}}\right)^3\left[\left(x_0^2+\frac{1}{2}\right)\cdot(1+\operatorname{erf} x_0)\frac{\sqrt{\pi}}{2}+x_0\,\mathrm{e}^{-x_0^2}\right]\right\}^{-1/2}, \tag{A1.2}$$

where erf stands for the error function and where $x_0 = \frac{r_0\sqrt{2}}{\sigma}$.

One has the following expression for the mean squared radius

$$\langle r^2\rangle = \frac{4\pi A^2\sigma^5}{4\sqrt{2}}\left\{\left(x_0^{3/2}+\frac{5x_0}{4}\right)\mathrm{e}^{-x_0^2} + \frac{\sqrt{\pi}}{2}\left(x_0^4+3x_0^2+\frac{3}{4}\right)(1+\operatorname{erf} x_0)\right\}. \tag{A1.3}$$

Similarly, one has

$$\langle p^2\rangle = \left\langle -\hbar^2\frac{\mathrm{d}^2}{\mathrm{d}r^2}\right\rangle = 4\pi\hbar^2A^2\sigma\left\{\frac{3}{8}\sqrt{\frac{\pi}{2}}+\frac{x_0}{4\sqrt{2}}\mathrm{e}^{-x_0^2}+\frac{1}{4}\frac{\sqrt{\pi}}{2}x_0^2 + \frac{3}{8}\sqrt{\frac{\pi}{2}}\operatorname{erf} x_0+\frac{1}{4}\sqrt{\frac{\pi}{2}}x_0^2\operatorname{erf} x_0\right\}. \tag{A1.4}$$

If $r_0 = 0$, one readily obtains

$$\langle r^2\rangle = \frac{3}{4}\sigma^2, \quad \frac{\langle p^2\rangle}{\hbar^2} = \frac{3}{\sigma^2}. \tag{A1.5}$$

This corresponds to the minimum spherical wave packet in three dimensions, as it should. One has indeed

$$\langle(\Delta\mathbf{r})^2\rangle = \langle r^2\rangle = \frac{3}{4}\sigma^2, \quad \langle(\Delta\mathbf{p})^2\rangle = \langle p^2\rangle = 3\frac{\hbar^2}{\sigma^2}, \tag{A1.6}$$

and

$$\langle(\Delta\mathbf{r})^2\rangle^{1/2}\langle(\Delta\mathbf{p})^2\rangle^{1/2} = 3\frac{\hbar}{2}. \tag{A1.7}$$

For x_0 or $\frac{r_0}{\sigma}$ very large, one obtains

$$\langle r^2\rangle = r_0^2+\frac{\sigma^2}{4}, \frac{\langle p^2\rangle}{\hbar^2} = \frac{1}{\sigma^2}, \tag{A1.8}$$

where only the leading terms have been retained. One now has

$$\langle(\Delta r)^2\rangle = \langle r^2\rangle - \langle r\rangle^2 = \frac{\sigma^2}{4}, \langle(\Delta p_r)^2\rangle = \langle p^2\rangle = \frac{\hbar^2}{\sigma^2}, \tag{A1.9}$$

and

$$\langle(\Delta r)^2\rangle^{1/2}\langle(\Delta p_r)^2\rangle^{1/2} = \frac{\hbar}{2}. \tag{A1.10}$$

Therefore, as $r_0 \to \infty$, the wave packet (A1.1) behaves as a minimum wave packet in one dimension (the radial one).

Appendix 2. Small time evolution of expectation values

Let us assume that we have a time dependent Hamiltonian. For simplicity we limit ourselves to the case of a linearly time-dependent potential

$$H = T + V_0 + \dot{V}t. \tag{A2.1}$$

We look for the small time expansion of the wave function

$$\psi = \psi_0 + \psi_1 t + \psi_2 \frac{t^2}{2} + \psi_3 \frac{t^3}{3!} + \ldots \tag{A2.2}$$

by plugging it into the Schrödinger equation. By simple algebra one obtains for the first terms

$$\psi_1 = \left(\frac{i\hbar}{2m}\Delta - \frac{iV_0}{\hbar}\right)\psi_0, \tag{A2.3}$$

$$\psi_2 = -\left(\frac{\hbar}{2m}\right)^2 \Delta^2\psi_0 + \frac{1}{2m}\Delta(V_0\psi_0) + \frac{1}{2m}V_0\Delta\psi_0 - \frac{V_0^2}{\hbar^2}\psi_0 + \frac{\dot{V}}{i\hbar}\psi_0, \tag{A2.4}$$

$$\begin{aligned}\psi_3 = {} & -i\left(\frac{\hbar}{2m}\right)^3 \Delta^3\psi_0 + i\frac{\hbar}{(2m)^2}[\Delta^2(V_0\psi_0) \\ & + \Delta(V_0\Delta\psi_0) + V_0\Delta^2\psi_0] \\ & - \frac{i}{2m\hbar^2}[\Delta(V_0^2\psi_0) + V_0\Delta(V_0\psi_0) \\ & + V_0^2\Delta\psi_0] + \frac{i}{\hbar^3}V_0^3\psi_0 \\ & - i\left(\frac{\hbar}{2m}\right)^3 \Delta^3\psi_0 + \frac{1}{2m}\Delta(\dot{V}\psi_0) + \frac{\dot{V}}{m}\Delta\psi_0.\end{aligned} \tag{A2.5}$$

We now calculate the expectation value of a Hermitian $\mathbf{r}$-dependent operator $O(\mathbf{r})$ as

$$\langle O\rangle = \langle O\rangle_0 + \alpha_1 t + \alpha_2\frac{t^2}{2} + \alpha_3\frac{t^3}{3!} + \ldots, \tag{A2.6}$$

where $\langle\ \rangle_0$ means an average over the initial wave function ψ_0. For α_1, we readily obtain

$$\alpha_1 = \frac{\hbar}{m}\mathrm{Im}\int \Delta\psi_0^* O\psi_0\, d^3r, \tag{A2.7}$$

which can be rewritten, after application of the divergence theorem

$$\alpha_1 = \int(\nabla O)\cdot\mathbf{j}(\mathbf{r})\, d^3r. \tag{A2.8}$$

The quantity $\mathbf{j}$ defined as

$$\mathbf{j} = \frac{\hbar}{m}\mathrm{Im}(\psi_0^*\nabla\psi_0) \tag{A2.9}$$

is nothing but as the initial Schrödinger current. For α_2, we obtain

$$\begin{aligned}\alpha_2 = {} & -2\left(\frac{\hbar}{2m}\right)^2\{\mathrm{Re}\int \Delta\psi_0^*\,\Delta O\,\psi_0\, d^3r \\ & + 2\,\mathrm{Re}\int\Delta\psi_0^*(\nabla O)\cdot(\nabla\psi_0)\, d^3r\} \\ & - \frac{1}{m}\int\psi_0^*(\nabla V_0)\cdot(\nabla O)\,\psi_0\, d^3r.\end{aligned} \tag{A2.10}$$

The general expression for α_3 is very long and not very transparent. For $V_0 = 0$, it reduces to

$$\begin{aligned}\alpha_3 = {} & 2\left(\frac{\hbar}{2m}\right)^2 \\ & \cdot\{\mathrm{Im}\int\psi_0^* O\Delta^3\psi_0\, d^3r - 3\,\mathrm{Im}\int\Delta\psi_0^* O\Delta^2\psi_0\, d^3r\} \\ & - \frac{1}{m}\mathrm{Re}\int\psi_0^*(\nabla O)\cdot(\nabla\dot{V})\psi_0\, d^3r.\end{aligned} \tag{A2.11}$$

For $O = r^2$, one obtains, up to $\mathcal{O}(t^2)$ terms, gathering (A2.6), (A2.7) and (A2.10)

$$\begin{aligned}\langle r^2\rangle = {} & \langle r^2\rangle_0 + 2[\int\mathbf{r}\cdot\mathbf{j}(r)\, d^3r]\, t \\ & + \left\{\frac{4}{m}\langle T\rangle_0 - \frac{2}{m}\langle\mathbf{r}\cdot\nabla V_0\rangle_0\right\}\frac{t^2}{2}.\end{aligned} \tag{A2.12}$$

It can be checked that all the remaining terms will involve the potential (V_0 or $\dot{V}$). Therefore for a free evolving wave packet, one has the exact result

$$\langle r^2\rangle = \langle r^2\rangle_0 + 2[\int\mathbf{r}\cdot\mathbf{j}(r)\, d^3r]\, t + \frac{2}{m}\langle T\rangle_0 t^2. \tag{A2.13}$$

For a real initial wave packet $\psi_0, \mathbf{j}$ vanishes and one then simply obtains

$$\langle r^2\rangle = \langle r^2\rangle_0 + \frac{2}{m}\langle T\rangle_0 t^2. \tag{A2.14}$$

We are interested in the case $V_0 = 0$, and ψ_0 real. Then $\alpha_1 = 0$ and the imaginary part in (A2.11) vanishes. One finally gets, up to the t^3 term

$$\langle r^2\rangle = \langle r^2\rangle_0 + \frac{2}{m}\langle T\rangle_0 t^2 - \frac{1}{3m}\langle(\nabla\dot{V})\cdot\mathbf{r}\rangle_0 t^3. \tag{A2.15}$$

For $O = r$, under the same conditions, one gets

$$\begin{aligned}\langle r\rangle = {} & \langle r\rangle_0 + \left(\frac{\hbar}{2m}\right)^2 \\ & \cdot\left[\int\Delta\psi_0\frac{2}{r}\psi_0\, d^3r + 2\int\Delta\psi_0\frac{\mathbf{r}}{r}\cdot\nabla\psi_0\, d^3r\right]t^2 \\ & - \frac{1}{6m}\left\langle(\nabla\dot{V})\cdot\frac{\mathbf{r}}{r}\right\rangle_0 t^3 + \ldots.\end{aligned} \tag{A2.16}$$

For the special case of a spherical wave packet, the quadratic term identically vanishes.

References

1. T. Matsui, H. Satz: Phys. Lett. 178 B (1986) 416
2. F. Karsch, R. Petronzio: Phys. Lett. 212 B (1988) 255
3. J.-P. Blaizot, J.Y. Ollitrault: Phys. Lett. 217 B (1989) 392
4. F. Karsch: Quark-gluon plasma signatures, p. 291. V. Bernard et al. (eds.). Gif sur Yvette: Edition Frontières 1991
5. A. Capella et al.: Phys. Lett. 206 B (1988) 354
6. C. Gerschel, J. Hüfner: Phys. Lett. 207 B (1988) 253
7. C. Gerschel, J. Hüfner: preprint 1992 Orsay IPNO-DRE 92-01, to be published
8. S. Gavin, M. Gyulassy, A. Jackson: Phys. Lett. 207 B (1988) 257
9. S. Gavin, M. Gyulassy: Phys. Lett. 214 B (1988) 241
10. V. Cerny et al.: Z. Phys. C46 (1990) 481
11. J. Cugnon, P.-B. Gossiaux: Europhys. Lett. 20 (1992) 31
12. F. Karsch: in: Quark-Gluon Plasma. R.C. Hwa (ed.), Advanced Series on Directions in High Energy Physics, vol. 6. Singapore: World Scientific 1990
13. J.L. Richardson: Phys. Lett. 82 B (1979) 272
14. J. Cleymans, R.L. Thews: Z. Phys. C45 (1990) 391
15. T. Matsui: Ann. Phys. 196 (1989) 182
16. J. Knoll et al.: Quark Matter 91, Gatlinburg, 1991; Nucl. Phys. A519 (1990) 831
17. L. Csernaï, J.I. Kapusta: preprint 1992 Minnesota TPI-MINN-92/10